Surface energy and magnetocapacitance of superconductors under electric field bias

K. Morawetz,[1,2] P. Lipavský,[3,4] J. Koláček,[4] and E. H. Brandt[5]
[1]*Forschungszentrum Rossendorf, Postfach 51 01 19, 01314 Dresden, Germany*
[2]*Max Planck Institute for the Physics of Complex Systems, Noethnitzer Strasse 38, 01187 Dresden, Germany*
[3]*Faculty of Mathematics and Physics, Charles University, Ke Karlovu 3, 12116 Prague 2, Czech Republic*
[4]*Institute of Physics, Academy of Sciences, Cukrovarnická 10, 16253 Prague 6, Czech Republic*
[5]*Max Planck Institute for Metals Research, D-70506 Stuttgart, Germany*
(Received 2 June 2008; published 27 August 2008)

A superconducting layer exposed to a perpendicular electric field and a parallel magnetic field is considered within the Ginzburg-Landau (GL) approach. The GL equation is solved near the surface and the surface energy is calculated. The nucleation critical field of superconducting state at the surface depends on the magnetic and electric fields. Special consideration is paid to the induced magnetic field effect caused by diamagnetic surface currents. The latter effect is strongly dependent on the thickness of the sample. The effective inverse capacitance determines the effective penetration depth. It is found that the capacitance exhibits a jump at the surface critical field. An experiment is suggested for determining the change in the effective capacitance of the layer.

DOI: 10.1103/PhysRevB.78.054525 PACS number(s): 74.25.Op, 74.25.Nf, 74.20.De, 85.25.−j

I. INTRODUCTION

The gate voltage can be used to change the carrier density of superconducting surfaces and therefore the critical temperature in the same manner as in field effect semiconductor devices. This effect has been investigated for more than 40 years[1] and has continuously gained experimental interest;[2–6] see also the overview.[7] The critical temperature of thin superconducting layers can be controlled in this way by an electric field applied perpendicular to the layer.[1,5,6,8,9] High-T_c superconductors are characterized by a low density of carriers such that this field effect is expected to be higher; this has caused a wide experimental activity.[2,3,10–13] Such field effect devices may be made even from organic and macromolecular films.[14]

According to the Anderson theorem, the bias voltage can change the critical temperature only indirectly via the electric field dependence of the material parameters.[4,15–20] The influence of the electric field on the pairing mechanism is therefore to be expected in the density of states for very pure and thin low-dimensional structures,[21–23] analogous to the formation of sidebands in the density of states due to high fields.[24] Capacitance measurements on surfaces of high-temperature superconductors have revealed a so far unknown mechanism for electric field penetration.[25]

On the other hand, magnetocapacitance techniques are used frequently to measure the influence of the magnetic field,[26] e.g., to test spin-dependent electrochemical potentials. Starting from the early reports on an increase in the capacitance[27] for superconducting tunneling junctions,[28] the residual surface resistance of superconducting resonators is still under discussion[29–31] since it becomes important for the question of how short the electron bunches can be in free-electron lasers before the generated wake fields disable the superconducting cavities.[30] Different mechanisms for such electron losses have been discussed in Ref. 31. With respect to this, it is important to know the explicit dependence on the magnetic field and the voltage bias.

In this paper we investigate the magnetocapacitance in dependence on the magnetic field and the external bias by the electric field. We focus on magnetic fields around the surface critical field B_{c3} since we expect that the external bias, which affects only the surface, has a relatively large effect on the surface superconductivity. Most experimental activities are concentrated on the change in the surface critical magnetic field with temperature.[32–37] In our study we suggest consideration of these measurements under the influence of external bias. To this end we will employ the Ginzburg-Landau (GL) equation with the de Gennes surface condition, where only the latter condition depends on the external bias, in agreement with the Anderson theorem.

The experimental setup is shown in Fig. 1. The first electrode of a capacitor is the superconducting slab of thickness d. It is sandwiched between two plates of an ideal metal at distances L, which form the second electrodes. In real devices it will be necessary to consider that the applied electric field affects also the end corners. Here we neglect the influence of the end corners, assuming an infinite plane capacitor. Our aim is to evaluate the effective capacitance, the surface critical field, and the surface energy in dependence on the applied voltage and the magnetic field.

The total energy of the capacitor with area S is given by $\frac{1}{2}\epsilon_0 E^2 LS$ and an additional contribution coming from surface

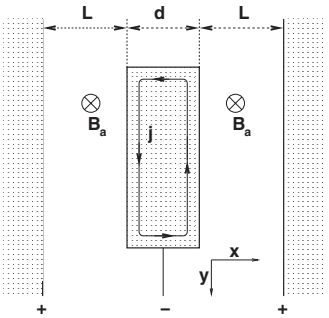

FIG. 1. The slab superconductor of thickness d placed in two parallel capacitor plates at distance L. The superconductor extends infinitely in the z direction. The magnetic field is parallel to the superconductor surface.

charges $S\sigma$. Then the inverse capacitance C of the slab is given by

$$\frac{S}{C} = \frac{L}{\epsilon_0} + \frac{1}{\epsilon_0^2}\frac{\partial^2\sigma}{\partial E^2}. \tag{1}$$

The external magnetic field associated with the z axis and parallel to the superconducting surface is screened inside the superconductor by the diamagnetic current $\mathbf{j}$. Thus a magnetic field profile is established perpendicular to the surface induced by the diamagnetic current. This induced diamagnetic current contributes to the inverse capacitance such that we have besides a genuine surface contribution $C_{\rm surf}$ also an induced part $C_{\rm ind}$,

$$\frac{1}{\epsilon_0^2}\frac{\partial^2\sigma}{\partial E^2} = \frac{S}{C_{\rm surf}} + \frac{S}{C_{\rm ind}}. \tag{2}$$

It will turn out that the induced capacitance is linearly dependent on the sample width d.

Since the electric field penetrates the superconductor only near the surface, it is of special interest to understand the surface superconductivity in the presence of an external electric field. The change in the upper critical field and the surface nucleation field has already been calculated for strong coupling.[38] The surface paraconductivity and the change in the critical parameters due to an external field has been investigated too.[39,40] A shift in the critical temperature has been obtained[41] due to a modified GL boundary condition and a variational solution of the effective Schrödinger equation. In other words, the critical field B_{c1} is changed due to the change in the GL energy by the electric field.[42] Here we will investigate the surface energy problem of domain walls similarly and employ the modified boundary condition to solve the GL equation variationally. We will obtain that the bulk critical field B_{c2} remains unchanged due to the applied electric field, while the surface critical field B_{c3} changes with the electric field.

The paper is organized as follows: First we repeat the solution of the magnetic field–dependent GL equation under external bias by electric fields and calculate the surface critical field B_{c3} and its dependence on the external bias. With the help of the GL wave function, the surface energy is calculated in Sec. III and the effective capacitance in Sec. IV. Special attention is paid to the induced magnetic field effect there. The self-consistent treatment of the induced magnetic field is presented in Appendix D 1, which completes the proposed picture. We present fitting formulas for the magnetic and electric field dependence aimed for experimental verifications. In Sec. V we summarize and discuss possible experimental realizations.

II. GL WAVE FUNCTION WITH EXTERNAL MAGNETIC AND ELECTRIC FIELDS

An effective description of superconducting properties near the critical temperature is provided by the GL equation for the wave function Ψ,

$$\frac{1}{2m}(-i\hbar\nabla - e\mathbf{A})^2\Psi + \alpha\Psi + \beta|\Psi|^2\Psi = 0, \tag{3}$$

which describes the ratio of the superconducting density to the total density n by $|\Psi|^2 = n_s/2n$. Here the mass is twice the electron mass, $m=2m_e$, and the charge is $e=2e_e$, the one of the Cooper pairs. The effective potential in GL equation (3), $\alpha\Psi+\beta|\Psi|^2\Psi$, is valid only near the critical temperature. If needed, the effective potential can be extended to temperatures lower than the critical one.[43,44]

The GL equation is supplemented by the de Gennes surface conditions[45]

$$\left.\frac{\nabla\Psi}{\Psi}\right|_{x=0} = \frac{1}{b}, \qquad \left.\frac{\nabla\Psi}{\Psi}\right|_{x=d} = -\frac{1}{b}, \tag{4}$$

where the extrapolation length b is sensitive to the treatment of the surfaces. The length b describes the extrapolation of the order parameter out of the surface when the restoring forces of the surface are neglected. Since the length b is real, it is assured that no current is flowing through the surface. Without external bias the typical length b_0 is on the order of a centimeter and can be neglected.[45]

This inverse extrapolation length $1/b$ depends on the density of states at the surface; therefore it is a function of the applied electric field E. In linear approximation (see Appendix A), it reads

$$\frac{1}{b} = \frac{1}{b_0} + \frac{E}{\varphi_{\rm fe}}, \tag{5}$$

with the characteristic potential[46]

$$\frac{1}{\varphi_{\rm fe}} = \frac{4e}{mc^2}\kappa^2\eta\frac{\partial \ln T_c}{\partial \ln n} \tag{6}$$

being on the order of a few MeV for conventional superconductors. The dependence of $1/\varphi_{\rm fe}$ on the GL parameter κ and the density derivative of the critical temperature suggests that the field effect is much larger for high-T_c superconductors.

The reduction factor η is the ratio of the gap extrapolated to the surface to the value at the surface.[46] Its value is on the order of unity and it is not essential for our discussion.

A. Nucleation of the surface superconductivity

At the surface critical field the superconductivity nucleates at the surface. Near the surface the effective wave function Ψ is small and we can work with the linearized GL equation, omitting in Eq. (3) the cubic term,

$$\frac{1}{2m}(i\hbar\nabla - e\mathbf{A})^2\Psi + \tilde{\alpha}\Psi = 0, \tag{7}$$

with boundary condition (4).

We consider the geometry of a planar superconductor at $d>x>0$ as in Fig. 1 and assume a homogeneous applied magnetic field $\mathbf{B}_a=(0,0,B_a)$. Since the system in Fig. 1 has translation invariance along the y direction, we use the Landau gauge of the form

$$\mathbf{A} = (0, B_a x, 0). \tag{8}$$

The nucleation is possible if the parameter $-\tilde{\alpha}$ in Eq. (7) becomes equal to an eigenvalue ε of the kinetic energy given by $\frac{1}{2m}(-i\hbar\nabla - e\mathbf{A})^2\psi = \varepsilon\psi$. Since α changes with the temperature, $\alpha = \alpha'(T - T_c)$, the eigenvalue ε of the kinetic energy determines the nucleation temperature T^* as $T^* - T_c = -\varepsilon/\alpha'$.[46] To avoid dual notation for the same quantity, we will treat Eq. (7) as an eigenvalue problem for $\tilde{\alpha}$. Since $\tilde{\alpha}$ is negative, the nucleation temperature T^* is always below the critical temperature T_c in the absence of the magnetic field.

Assuming the translation invariance along the y and z axes, we can write the wave function as

$$\Psi(x,y,z) = \psi(x)e^{iky}e^{iqz}. \tag{9}$$

Using Eq. (9) in GL equation (7), we get a one-dimensional equation,

$$\frac{\hbar^2}{2m}\left[-\left(\frac{\partial}{\partial x}\right)^2 + \left(k - \frac{eB_a}{\hbar}x\right)^2 + q^2\right]\psi + \alpha\psi = 0. \tag{10}$$

Any nonzero value of q results in the kinetic energy $q^2\hbar^2/2m$, which lowers the value of α, making the nucleation temperature lower. The nucleation happens on the first possible occasion, i.e., at the highest allowed temperature. We thus take $q=0$.

The value of k determines the minimum of the parabolic potential and the eigenvalue α depends on the relative position of this minimum with respect to the surface of the slab. We have to find the wave vector k from the requirement of the highest nucleation temperature.

B. Thick slab limit

First, we assume that the superconducting slab is so thick that its surface superconductivity forms on both surfaces independently. In this case we can view the sample as infinite and take the convergent solution into the bulk. We treat only the surface at $x=0$. The surface at $x=d$ is analogous. We should note that the profile for a general thickness has been solved by a calculation based on the Eilenberger equation for finite temperatures but without bias voltage.[47] Here we restrict ourselves to a simpler approach but include the bias voltage.

It is advantageous to express the x coordinate with the help of the dimensionless coordinate τ,

$$x = \tau l + 2l^2k, \tag{11}$$

such that the wave function reads

$$\psi(x) = \mathcal{C}D_{\tilde{\nu}}\left(\frac{x}{l} + \tau_0\right), \tag{12}$$

with the momentum $\tau_0 = -2kl$ and the magnetic length

$$l^2 = \frac{\hbar}{2eB_a}. \tag{13}$$

The parabolic cylinder function $D_\nu(\tau)$ solves differential equation (7), i.e.,[48]

$$\frac{d^2D_\nu(\tau)}{d\tau^2} = \left(\frac{\tau^2}{4} - \nu - \frac{1}{2}\right)D_\nu(\tau), \tag{14}$$

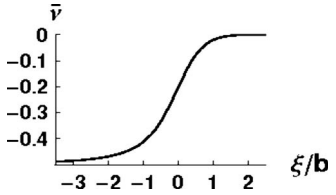

FIG. 2. The minimal eigenvalue of the GL equation given by Eq. (17) as a function of external bias.

$$\left.\frac{D'_\nu(\tau_0)}{D_\nu(\tau_0)}\right|_{\tau_0 = -k\sqrt{2\hbar/eB_a}} = \frac{l}{b}, \tag{15}$$

with

$$\nu = -\frac{1}{2} - \frac{\alpha m}{e\hbar B_a} \tag{16}$$

and the GL coherence length $\xi^2 = -\hbar^2/2m\alpha$.

Boundary condition (15) leads to a function $\nu(\tau_0)$. The maximal nucleation temperature is given by the maximal $\tilde{\alpha} = \max[\alpha]$, which is characterized by the minimum $\tilde{\nu} = \min[\nu(\tau_0)]$ due to Eq. (16). Besides the obvious numerical search, we can give directly a nonlinear equation for this desired minimum $\tilde{\nu}'(\tau_0) = 0$. For this purpose we differentiate Eq. (15) with respect to τ_0, using the relations for the parabolic cylinder functions, $D'_\nu = \tau D_\nu/2 - D_{\nu+1}$ and $D_{\nu+1} = \tau D_\nu - \nu D_{\nu-1}$, to arrive at

$$\left.\frac{D_{\tilde{\nu}+1}(\tau_0)}{D_{\tilde{\nu}}(\tau_0)}\right|_{\tau_0 = -2\sqrt{(\tilde{\nu}+1/2)(1+\xi^2/b^2)}} = -\sqrt{\left(\tilde{\nu} + \frac{1}{2}\right)\left(1 + \frac{\xi^2}{b^2}\right)} - \frac{\xi}{b}\sqrt{\tilde{\nu} + \frac{1}{2}}. \tag{17}$$

With the solution $\tilde{\nu}[\tau_0]$ of Eq. (17), the momentum and current is determined due to $\tau_0 = -2kl$. In Fig. 2 the solution of Eq. (17) is plotted. There is an asymmetry to be noted with respect to positive, $b>0$, and negative, $b<0$, external biases. This will lead to very asymmetric curves in the surface energy later.

C. Surface critical field

The lowest eigenvalue $\tilde{\nu} = \min[\nu(\tau_0)]$ of Eq. (14) corresponds to the highest attainable critical magnetic field

$$B_{c3} = \max(B_a) = \frac{-m\alpha}{\hbar e\left(\tilde{\nu} + \frac{1}{2}\right)} \equiv \frac{B_{c2}}{2\tilde{\nu} + 1}, \tag{18}$$

where B_{c2} is the upper critical field. The modified boundary condition does not influence B_{c2} but makes it possible that $-1/2 < \tilde{\nu} \leq 0$ and a higher critical magnetic field $B_{c3} > B_{c2}$ appears such that the superconductivity near the surface is enhanced in dependence on the external electric field.

In Fig. 3 we present the result for surface critical field (18) versus external bias (4). We see that the external bias can enhance or decrease the surface critical value depending on the field direction. Without external bias and at $1/b_0 = 0$,

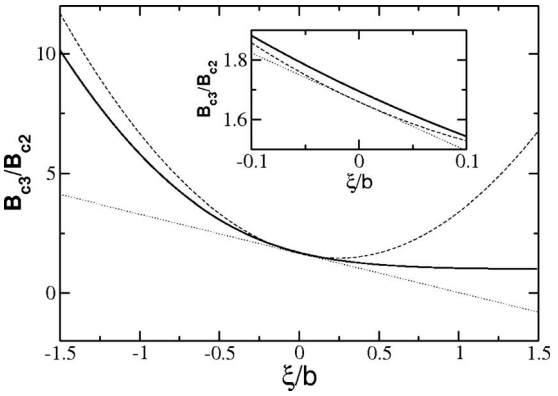

FIG. 3. The surface critical field B_{c3} versus external bias (4) from linearized GL equation. Solution (18) (solid line) is compared with the expansion up to first (dotted line) and second (dashed line) order in $1/b$ according to Eq. (20). The inset enlarges the area around zero external bias.

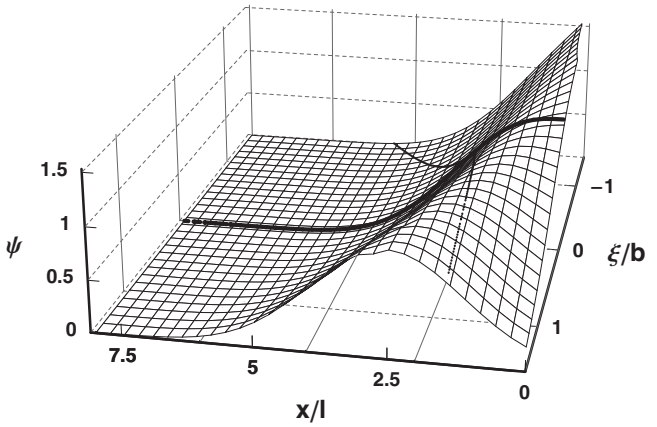

FIG. 4. The GL wave function of the condensate versus external bias (4). The normal GL wave function without external bias is marked as a thick line. The transition curve of ξ/l at $B_a=B_{c3}$ according to Eq. (21) is plotted as a dotted line.

the known GL solution $B_{c3}/B_{c2}=1.694\,61$ is reproduced.[49] The strong coupling limit is somewhat larger, resulting in the value of 1.8.[38] We see that the electric field can generate easily a value larger than 1.695. The experimental values compared with the GL theory and the theory of Hu and Korenman[33] are discussed in Ref. 50, which shows that the GL values are too small.

To provide analytical expressions, let us recall a simpler variational solution of the problem which was contributed by Kittel for absent external bias.[45,51] We can extend this approach to external voltage bias and choose for the wave function the *ad hoc* ansatz $\psi \approx \mathcal{C}\exp(-ax^2+x/b)$, which obeys the de Gennes boundary condition $\psi'/\psi|_0=1/b$ automatically. The constants a and $\tau_0=-2kl$ have to be determined by the minimal eigenvalue of Eq. (7). The normalized minimal mean eigenvalue $\langle\tilde{\alpha}\rangle$ can be obtained by minimizing the functional

$$\langle\tilde{\alpha}\rangle = \frac{\int_0^\infty dx[l_{\min}^{-4}(x+\tau_0 l)^2\phi^2 - \phi''\phi]}{\int_0^\infty dx\phi^2} \tag{19}$$

with respect to τ_0 and a. The resulting $l_{\min}^{-2}=2eB_{c3}/\hbar$ yields

$$\frac{B_{c3}}{B_{c2}} \equiv \frac{\xi^2}{l_{\min}^2} = \sqrt{\frac{\pi}{-2+\pi}} - \frac{2}{(-2+\pi)^{3/2}}\frac{\xi}{b} + \frac{\{21+2\pi[2+(-4+\pi)\pi]\}}{2(-2+\pi)^{5/2}\sqrt{\pi}}\frac{\xi^2}{b^2} + \mathcal{O}\left(\frac{1}{b^3}\right). \tag{20}$$

In the case of vanishing electric fields corresponding to the boundary condition $1/b \approx 0$, we recover the known results,[51] $a=1/2\xi^2$, $x_0=1/\sqrt{2\pi a}$, and $B_{c3}/B_{c2}=\sqrt{\pi/(\pi-2)}\approx 1.66$. The comparison of expansion (20) with solution (18) can be seen in Fig. 3.

D. Variational wave function

Let us now return to the full solution of Eq. (10). The wave function (12) specified by the value $\nu=\tilde{\nu}$ describes the situation for the maximal nucleation temperature corresponding to the maximal magnetic field $B_a \approx B_{c3}$.

In Fig. 4 we see how the external bias $1/b$ changes the wave function in dependence on the distance of the surface. The magnetic field enters merely as a scaling of the spatial coordinate. For positive electric fields the superconducting density is diminished on the surface, while for oppositely directed electric fields the surface superconductivity is enhanced.

Since the wave function is strictly valid only near the transition line $B_a \approx B_{c3}$, we have also plotted in Fig. 4 the transition line

$$\left.\frac{\xi}{l}\right|_{B_a=B_{c3}} = \frac{1}{\sqrt{\tilde{\nu}+\frac{1}{2}}} \tag{21}$$

for $x=\xi$ as orientation.

We will use wave function (12) as an ansatz for the variational calculation of the surface energy in such a way that the amplitude $\mathcal{C}$ serves as a variational parameter. This is motivated by the fact that near the surface, the shape of the wave function is only slightly changed compared to the surface values but the amplitude decreases exponentially away from the surface.

III. SURFACE ENERGY

With the help of the GL wave function, we can now calculate the surface energy. This surface energy is the integral over the energy difference between the actual Gibbs free energy and the Gibbs free energy deep in the superconductor. Since the latter equals the one deep in the normal region when the field energy is subtracted, $G(x\to-\infty)=G_{n0}-B_a^2/2\mu_0=G_{s0}$, we can write the surface energy as

$$\sigma = \int_0^\infty dx \left[G(x) - G_{n0} + \frac{B_a^2}{2\mu_0} \right] = \int_0^\infty dx [G(x) - G_{s0}]$$
$$= \int_0^\infty dx \left[\alpha |\Psi|^2 + \frac{\beta}{2} |\Psi|^4 + \frac{[B_a - B(x)]^2}{2\mu_0} + \frac{|(i\hbar \nabla + e\mathbf{A})\Psi|^2}{2m} \right] + \frac{\hbar^2}{2m} \Psi(0)\Psi'(0). \quad (22)$$

The last counterterm is necessary in order to provide a consistent variational problem with modified GL boundary condition (4); for details see Appendix B.

The surface energy appears only if terms $\sim|\Psi|^4$ are taken into account. Since the shape of the GL wave function changes much less in terms of the applied magnetic field than the amplitude does, we can now use our solution of the linearized equation, $\Psi = \mathcal{C} D_{\tilde{\nu}}$, to calculate the surface energy. For this purpose we determine the constant N,

$$\mathcal{C}^2 = N \frac{\alpha}{\beta}, \quad (23)$$

such that Eq. (22) takes a minimum.

A. Limit of thick samples

Assuming the limit of thick sample, $d \gg l$, we neglect in the first step the space profile of the magnetic field near the surface. This profile or induced field effect due to diamagnetic currents will be discussed separately in the next paragraph. In the same spirit, the upper integration limit is taken as infinite here at this moment. Nonlinear Gibbs free energy (22) then reads

$$G = G_0 - l \frac{B_c^2}{2\mu_0} (2N\mathcal{A} - N^2 \mathcal{B}). \quad (24)$$

Here we have introduced

$$\mathcal{A} = \int_{\tau_0}^\infty d\tau \left\{ \left(\frac{\tau^2 \xi^2}{4l^2} - 1 \right) D_{\tilde{\nu}}^2(\tau) + \frac{\xi^2}{l^2} [D'_{\tilde{\nu}}(\tau)]^2 \right\} + \frac{\xi^2}{l^2} D_{\tilde{\nu}}(0) D'_{\tilde{\nu}}(0) = -\left(1 - \frac{\tilde{\alpha}}{\alpha} \right) \int_{\tau_0}^\infty d\tau D_{\tilde{\tau}}^2(\tau),$$

$$\mathcal{B} = \int_{\tau_0}^\infty d\tau D_{\tilde{\nu}}^4(\tau) \quad (25)$$

and used $\alpha^2/\beta = B_c^2/\mu_0$. The minimum of Eq. (24),

$$N = \mathcal{A}/\mathcal{B}, \quad (26)$$

leads to a surface energy σ in terms of the condensation energy expressed in the critical field

$$\sigma = \frac{B_c^2}{2\mu_0} \delta(b), \quad (27)$$

with the wall parameter

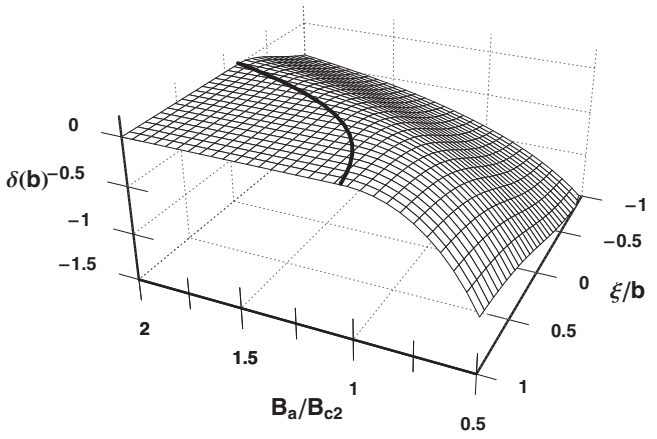

FIG. 5. The surface energy in terms of wall parameter (28) versus the magnetic field and the external bias $1/b$. The solid line denotes the transition curve $B_a = B_{c3}$ according to Eq. (21), where the surface energy vanishes.

$$\delta(b) = -l \frac{\mathcal{A}^2}{\mathcal{B}}. \quad (28)$$

In Fig. 5 the wall parameter is plotted versus the external bias and the magnetic length. We see that with increasing magnetic fields, i.e., decreasing magnetic length, the negative surface energy increases dependently on the external bias. Therefore the surface energy can be changed by the applied magnetic field as well as the external bias. The line of minimal eigenvalues of GL equation (21) called transition curve is shown as well, where $B_a = B_{c3}$ and the surface energy vanishes.

It is instructive to derive the wall parameter for the case without external bias,

$$\delta(\infty) = -l \left[\frac{\xi^2}{l^2} \left(\tilde{\nu} + \frac{1}{2} \right) - 1 \right]^2 \mathcal{D} = -\lambda \sqrt{\frac{B_c}{B_a}} \frac{\left[(2\tilde{\nu} + 1) \sqrt{\frac{B_a}{B_c}} - \sqrt{2\frac{B_c}{B_a}} \kappa \right]^2}{(\sqrt{2}\kappa)^{5/2}} \mathcal{D}, \quad (29)$$

with

$$\mathcal{D} = \left[\int_{\tau_0}^\infty d\tau D_{\tilde{\nu}}^2(\tau) \right]^2 / \int_{\tau_0}^\infty d\tau D_{\tilde{\nu}}^4(\tau). \quad (30)$$

The upper critical field is related to the GL parameter $B_{c2} = \sqrt{2}\kappa B_c$ and $l^2/\xi^2 = B_{c2}/2B_a$. With the help of Eq. (18), it is also easy to check that surface energy (29) is exactly zero for $B_a = B_{c3}$ in the case of absent external bias.

Assuming magnetic fields $B_a \approx B_c$ in order to adapt to the situation of the superconductor-normal surface-wall parameter, we obtain

$$\lim_{B_a \to B_c} \delta(\infty) = -\lambda \frac{2.032}{\kappa^{5/2}} (0.417\,27 - \kappa)^2. \quad (31)$$

An approximate treatment of the wall parameter of the superconductor-normal region is presented in Appendix C.

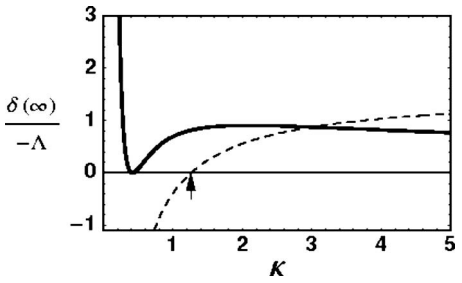

FIG. 6. Surface-wall parameter (29) for superconductor-vacuum boundary and zero external bias (31) versus the GL parameter (solid line) compared to the superconductor-normal boundary expression [Eq. (32)] in the literature (dotted line).

Neglecting induced diamagnetic currents, the wall parameter δ for both type-I and type-II superconductors[45,51,52] is approximated by Eq. (C8),

$$\delta_{s\text{-}n} \approx -\lambda\left(\frac{3}{2} - \frac{4\sqrt{2}}{3\kappa}\right), \tag{32}$$

in terms of the London penetration depth λ of the magnetic field and the GL parameter $\kappa=\lambda/\xi$ with the coherence length ξ.

Result (31) for the superconductor-vacuum transition can be compared with this superconductor-normal boundary [Eq. (32)]. In Fig. 6 we plot Eqs. (31) and (32) and in this one sees the different places where the surface energy vanishes. This vanishing of surface energy is connected with the transition from type-I to type-II superconductivity. In the latter case the surface energy is negative, indicating an unstable surface forming a vortex structure. While the superconductor-normal result [Eq. (32)] leads to

$$\kappa_0|_{s\text{-}n} = 8\sqrt{2}/9 = 1.257, \tag{33}$$

the superconductor-vacuum result [Eq. (31)] suggests a smaller value,

$$\kappa_0|_{s\text{-}v} = \frac{2\tilde{\nu}+1}{\sqrt{2}} = 0.417\ 27. \tag{34}$$

Without external magnetic field, $\tilde{\nu}=0$, the superconductor-vacuum result [Eq. (31)] coincides with the transition point between type-I and type-II superconductivities. In other words the superconductor-vacuum boundary leads to smaller values of the transition between type I and type II than those for the superconductor-normal boundary with respect to the stability of the surfaces. We find that the applied magnetic field decreases the transition GL parameter. The type-II superconductivity extends toward values below $\kappa=1/\sqrt{2}=0.7071$.

B. Finite width of samples

When the applied magnetic field B_a exceeds the upper critical field B_{c2}, no bulk superconductivity is possible anymore except in a small surface region. The surface superconductivity occurs up to the surface critical field B_{c3}. This critical field is dependent on the thickness of the sample.[47] We have discussed so far the thick sample limit with respect to London's penetration depth, $d \gg \lambda$. Now we are going to consider the finite sample limit.

Investigating a layer of finite thickness, $d<\infty$, Gibbs free energy (24) with Eq. (25) possesses an upper integration limit $d/l+\tau_0$ instead of ∞. The superconducting surfaces are then also characterized by the appearance of diamagnetic currents. These diamagnetic currents induce magnetic fields; see Appendix D. These fields contribute to the surface energy. We solve again the variation problem of Gibbs free energy (24) in order to obtain the optimum $\mathcal{C}$. The expression for the surface energy [Eq. (22)] remains the same but the magnetic profile is now spatially dependent,

$$B(x) = B_a + \mu_0 M(x). \tag{35}$$

The explicit form of the external magnetic field cancels in the Gibbs energy and is present only in the vector potential, which now takes form (D6),

$$A_y(x) = B_a x + \mu_0 \int_0^x dx' M(x'), \tag{36}$$

instead of Eq. (8). As a result, Eq. (24) assumes

$$\begin{aligned} G = G(M=0) - l\frac{B_c^2}{2\mu_0}\Bigg\{ & \frac{N}{\sqrt{2}\kappa}\int_{\tau_0}^{d/l+\tau_0} d\tau D_{\tilde{\nu}}(\tau)^2 \\ & \times \left[\frac{B_c}{B_a}\left(\int_{\tau_0}^{\tau} d\tau' \frac{\mu_0 M(\tau')}{B_c}\right)^2 + 2\tau\int_{\tau_0}^{\tau} d\tau' \frac{\mu_0 M(\tau')}{B_c}\right] \\ & - \int_{\tau_0}^{d/l+\tau_0} d\tau\left(\frac{\mu_0 M(\tau)}{B_c}\right)^2\Bigg\} \\ = & -\frac{lB_c^2}{2\mu_0}[2N\mathcal{A} - N^2(\mathcal{B}+\mathcal{B}') + \mathcal{D}'N^3] + \mathcal{O}(N^4). \end{aligned} \tag{37}$$

Here we have used Eq. (D13) in the last line. Besides Eq. (25), we now obtain additional integrals, $\mathcal{B}'$ given by Eq. (E7) and $\mathcal{D}'$ by Eq. (E17) calculated in Appendix E.

Gibbs free energy (37) now contains now terms $\sim\mathcal{C}^6$ and the minimization yields a quadratic equation for $\mathcal{C}^2$. Instead of Eq. (26), we have

$$N = \frac{\mathcal{A}}{\mathcal{B}+\mathcal{B}'}\frac{1}{\mathcal{Y}}(1-\sqrt{1-2\mathcal{Y}}), \tag{38}$$

with

$$\mathcal{Y} = 3\frac{\mathcal{A}\mathcal{D}'}{(\mathcal{B}+\mathcal{B}')^2}. \tag{39}$$

The resulting surface energy takes the form of Eq. (27) with the wall parameter

$$\delta_{\text{ind}}(b) = -l\frac{\mathcal{A}^2}{\mathcal{B}+\mathcal{B}'}g(\mathcal{Y}) \tag{40}$$

and

$$g(x) = \frac{2}{3x^2}[3x-1+(1-2x)^{3/2}] \approx 1 + \frac{x}{3} + \cdots. \tag{41}$$

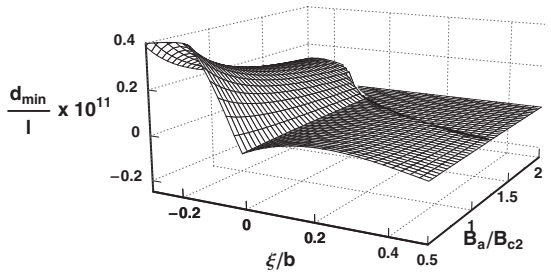

FIG. 7. The minimal thickness of the sample considered within the present approach versus the applied magnetic field and the external bias $1/b$ in units of the coherence length ξ. The transition line according to Eq. (21) is given as well.

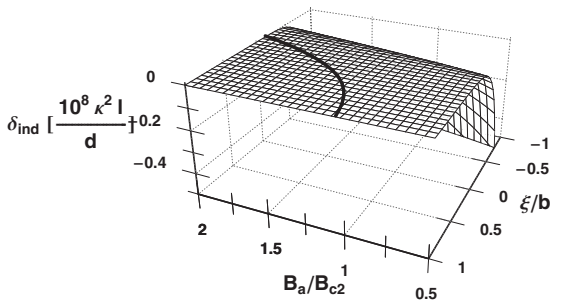

FIG. 8. The induced part of surface energy (43) in terms of wall parameter (28) versus the magnetic field and the external bias $1/b$. The solid line denotes the transition curve $B_a=B_{c3}$.

From Eq. (38) we see that the variational solution is meaningful only if $\mathcal{Y}<1/2$. This specifies the lower limit on the thickness $d_{\min}$ of our sample we can consider within this approximation. From Eq. (39) and with the help of Eqs. (E7) and (E17), we obtain

$$d_{\min} > \frac{12\mathcal{A}\mathcal{J}}{\mathcal{F}^3}\frac{l^3}{\xi^2} + \mathcal{O}(d^{-1}), \tag{42}$$

where $\mathcal{F}$ is given by Eq. (E9) and $\mathcal{J}$ by Eq. (E18). This lower limit is plotted in Fig. 7 in terms of the magnetic length. One sees that we have practically a visible lower limit only for strong negative values of the external bias.

Limit toward large sample thickness

It is now interesting to discuss the limit of thick superconductor probes. As shown in Appendix E, both expressions $\mathcal{B}'$ and $\mathcal{C}'$ are linearly dependent on the thickness d. We obtain for wall parameter (40)

$$\delta_{\text{ind}}(b) = -\frac{2\kappa^2 l^2 \mathcal{A}^2}{\mathcal{F}^2 d} + \mathcal{O}(d^{-2}), \tag{43}$$

where $\mathcal{F}$ is given by Eq. (E9), see Fig. 8. In the case of absent external bias, one has

$$\delta_{\text{ind}}(\infty) = -\frac{2\kappa^2 l^2}{d\langle x\rangle^2}\left[\frac{\xi^2}{l^2}\left(\tilde{\nu}+\frac{1}{2}\right)-1\right]^2 = -\frac{\lambda\xi}{d\langle x\rangle^2\sqrt{2}}\left[(2\tilde{\nu}+1)\sqrt{\frac{B_a}{B_c}}-\kappa\sqrt{2\frac{B_c}{B_a}}\right]^2, \tag{44}$$

with $\xi^2/l^2 = 2B_a/B_{c2}$, $B_{c2}=\sqrt{2}\kappa B_c$, and the mean distance

$$\langle x\rangle = \int_{\tau_0}^{d/l+\tau_0} d\tau\tau D_{\tilde{\nu}}^2(\tau) \Big/ \int_{\tau_0}^{d/l+\tau_0} d\tau D_{\tilde{\nu}}^2(\tau). \tag{45}$$

If $B_a \approx B_c$, we have

$$\lim_{B_a\to B_c} \delta_{\text{ind}}(\infty) = -744\ 326\frac{\lambda\xi}{d}(0.417\ 27-\kappa)^2. \tag{46}$$

We see that the surface energy vanishes at the same GL parameter as without induced fields [Eq. (31)].

IV. EFFECTIVE CAPACITANCE

Now we return to the experimental setup in Fig. 1 and determine the expected contributions to effective capacitance (1). Besides the ideal capacitance, $C_0=\epsilon_0 S/L$, we obtain contributions due to the external bias,

$$\frac{S}{C_{\text{ex}}} = \frac{1}{\epsilon_0^2}\frac{\partial^2\sigma}{\partial E^2} = \frac{\xi^2}{\epsilon_0^2\varphi_{\text{el}}^2}\frac{\partial^2\sigma}{\partial(\xi/b)^2} = \frac{L_0}{\epsilon_0}\frac{l}{\xi}\frac{\partial^2}{\partial(\xi/b)^2}\left(\frac{\delta}{l}\right)4(1-t)^2 = 4(1-t)^2\left.\frac{S}{C_{\text{ex}}}\right|_0, \tag{47}$$

where the temperature dependence $t=T/T_c$ arises from $B_c^2/2\mu_0=(\epsilon_c/n)(1-t^2)^2$ and $\kappa^2(T)=2\kappa^2/(1+t^2)$ in Eq. (6) and we have scaled with respect to the temperature-independent coherence length $\xi=\xi(T)\sqrt{1-t^2}$ and φ_{el} in Eq. (6). We abbreviate

$$\frac{L_0}{\epsilon_0} = \frac{\xi^3}{\epsilon_0^2\varphi_{\text{el}}^2}\frac{B_c^2}{2\mu_0} = \frac{\epsilon_c}{ne\kappa_0^3}\left(\frac{mc^2}{e}\right)^{3/2}\frac{1}{\sqrt{ne\epsilon_0}}\frac{1}{\varphi_{\text{el}}^2|_{t=0}}. \tag{48}$$

Using the BCS expression for the GL parameter $\beta = 24\hbar^2/7\zeta[3]nm(1.76)^2\xi_{\text{BCS}}^2$, we can rewrite Eq. (48) into another form also,

$$\frac{L_0}{\epsilon_0} = \alpha_0^4\frac{7\pi\zeta[3]}{6}a_B^3 n\left(1.76\kappa^2\eta\frac{\partial \ln T_c}{\ln n}\right)^2\sqrt{\tilde{\nu}+\frac{1}{2}}\frac{\xi_{\text{BCS}}^2}{\epsilon_0 l}, \tag{49}$$

with Bohr radius a_B and the Sommerfeld constant α_0.

The contribution due to the external bias consists now of two contributions,

$$\frac{1}{C_{\text{ex}}} = \frac{1}{C_{\text{surf}}} + \frac{1}{C_{\text{ind}}}, \tag{50}$$

according to the thick sample limit of surface energy, Eqs. (27) and (28), and the induced contribution due to diamagnetic currents, Eq. (40). In the following we will discuss them separately.

A. Limit of thick samples

With the help of the surface energy shown in Fig. 5, we can calculate the surface part of inverse capacitance (50), which is seen in Fig. 9. The larger the magnetic field is, the

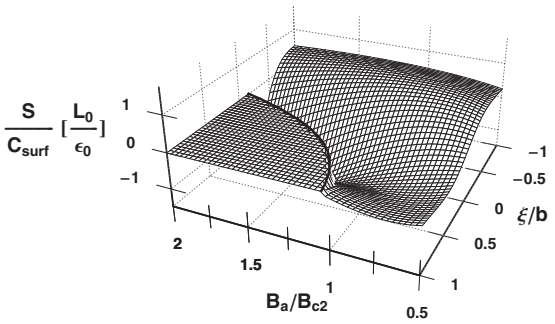

FIG. 9. The effective change in inverse capacitance in terms of Eq. (48) versus the magnetic field and the external bias $1/b$ in units of the coherence length ξ. The transition line is plotted as in Fig. 8.

larger is the inverse capacitance. For orientation we have plotted the transition line of the minimal eigenvalue of the GL equation where the surface energy vanishes.

In order to provide easy to use formulas, we can fit in terms of Eq. (48) to obtain

$$\left.\frac{S}{C_{\mathrm{surf}}}\right|_0 = \frac{L_0}{\epsilon_0}\left(\frac{l}{\xi}\right)^{3.25} h\left(\frac{\xi}{b}\right), \tag{51}$$

with

$$h(x) = 1.72(x-0.39)\mathrm{e}^{-2.20(x-0.39)^2}. \tag{52}$$

Using as an estimate the parameters in Table I, one finds for pure Nb $L_0/\epsilon_0(t=0)=0.248$ nm^2/pF, while for the $YBa_2Cu_3O_7$ one gets $L_0/\epsilon_0(t=0)=2.547$ nm^2/fF. This means that the expected change in the inverse capacitance would be some nm^2/pF. This should be compared to the trivial part of the inverse capacitance L/ϵ_0. Measuring the distance L between the capacitor and the superconductor in millimeters, one obtains $L/\epsilon_0=112.9(L/\mathrm{mm})$ nm^2/pF such that a relative precision of 10^3 should be required to resolve experimentally the measured effect.

B. Finite width of samples

Now we focus on the induced effect by diamagnetic currents. The contribution to effective capacitance (50) calculated from Eq. (43) is plotted in Fig. 10. Comparing this to Fig. 9, one sees a different shape. Dependent on the size of the sample, the induced effect can be larger than the thick sample limit.

The induced effect [Eq. (44)] can be fitted analogously to Eq. (51) as

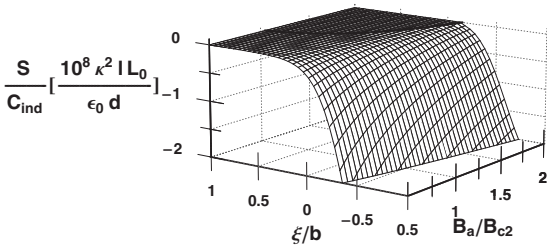

FIG. 10. The induced part of the effective inverse capacitance in units of the inverse sample thickness scaled with $\kappa^2\xi$. The transition line is plotted as in Fig. 8.

$$\left.\frac{S}{C_{\mathrm{ind}}}\right|_0 = \frac{\kappa^2 l}{d}\frac{L_0}{\epsilon_0}\left(\frac{l}{\xi}\right)^{3.25} h_{\mathrm{ind}}\left(\frac{\xi}{b}\right), \tag{53}$$

with

$$h_{\mathrm{ind}}(x) = -0.028e^{-0.46(x-0.19)^2}(0.19+0.43x-1.5x^2-0.16x^3 + x^4), \tag{54}$$

valid for $\xi/b<1.5$.

It is interesting to observe that both results, the external [Eq. (28)] as well as the induced one [Eq. (43)], show a nearly quadratic dependence,

$$C \sim l^4 \sim B_a^{-2}, \tag{55}$$

on the external magnetic field. This qualitative dependence on the magnetic field has been observed in magnetocapacitance measurements.[26]

V. SUMMARY AND CONCLUSION

In this paper we have considered a superconducting layer under the influence of external magnetic fields parallel to the surface and an electric field perpendicular to the surface. We found a nonlinear dependence of the surface critical magnetic field and the surface energy on the magnetic and electric fields. An effective capacitance is introduced, which allows measurement of these field effects. The diamagnetic currents induce a magnetic field profile. The self-consistent equation for the induced magnetization in terms of a superconducting density profile is derived. The induced magnetization represents an important contribution to the surface energy and the effective capacitance. We report an explicit dependence of the surface energy and the effective capacitance on the layer thickness. The inversely linear dependence on the thickness as well as the nearly quadratic dependence on the magnetic field of the inverse capacitance is in quali-

TABLE I. Used material parameters.

	ϵ_c/n (μeV)	κ_0	n (10^{28} m^{-3})	$\frac{\partial \ln T_c}{\partial \ln n}$	$\frac{\partial \ln \gamma}{\partial \ln n}$	$1/\varphi_{\mathrm{el}}$ (1/MV)	L_0/ϵ_0 (nm^2/pF)
Nb	4.585	0.78	2.2	0.74[a]	0.42[a]	4.52	0.248
$YBa_2Cu_3O_7$	750	55	0.5	−4.82[b]	−4.13[b]	−207.5	2547

[a]Reference 44.
[b]Reference 53.

tative agreement with measurements of magnetocapacitance. We predict a similar behavior to be valid also in capacitor measurements on superconductors. The effective capacitance is found to show a jump at the surface critical field. An experimental setup of such capacitance measurements supplemented by fit formulas is suggested.

ACKNOWLEDGMENTS

This work was supported by Research Plans of Czech Republic No. MSM 0021620834 and No. AVOZ10100521, by Grants No. GAČR 202/07/0597, No. GAČR 202/08/0326, and No. GAAV 100100712, by German PPP project of DAAD, by DFG Priority Program 1157 via Grant No. GE1202/06 and the BMBF, and by European ESF program NES.

APPENDIX A: DERIVATION OF MODIFIED GL BOUNDARY CONDITIONS

Let us outline the appearance of modified boundary condition (4). Therefore we start with the standard GL equation [Eq. (3)],

$$\frac{1}{2m}(-i\hbar\nabla - e\mathbf{A})^2\tilde{\Psi} + \alpha\tilde{\Psi} + \beta|\tilde{\Psi}|^2\tilde{\Psi} = 0, \tag{A1}$$

supplemented by the standard GL boundary condition that no current flows through the surface,

$$\mathrm{Im}\left[\frac{(i\hbar\nabla + e\mathbf{A})\tilde{\Psi}}{\tilde{\Psi}}\right]_{x=0} = 0. \tag{A2}$$

The electric field will change the material parameters, i.e., the GL parameters α and β. Linearizing GL equation (A1) with respect to this induced electric field effect results in $\tilde{\Psi}=\Psi+\delta\Psi$, where Ψ obeys GL equation (A1) but with different boundary condition. To see this, we assume that the induced part of the wave function, which is written as $\delta\Psi = \Psi\bar{\Psi}$ (where $\bar{\Psi}$ is proportional to the square of the Thomas-Fermi screening length[54]), is very small[54] such that its explicit influence can be disregarded. However it affects the boundary condition, which translates now from Eq. (A2) for $\tilde{\Psi}$ into the form for Ψ,

$$\mathrm{Im}\left[\frac{(i\hbar\nabla - e\mathbf{A})\Psi}{\Psi}\right]_{x=0} = -\left.\frac{\nabla\bar{\Psi}}{1+\bar{\Psi}}\right|_{x=0}. \tag{A3}$$

Since $\bar{\Psi}\sim E$, the external bias changes the boundary condition of the GL equation into the form

$$\mathrm{Im}\left[\frac{(i\hbar\nabla - e\mathbf{A})\Psi}{\Psi}\right]_{x=0} = \frac{1}{b_0} + \frac{E}{\varphi_{\mathrm{fe}}} \equiv \frac{1}{b} \tag{A4}$$

in linear order of the external bias. Since the vector potential is real in our case, we obtain Eq. (4). The explicit form [Eq. (4)] has been derived[46] for layered superconductors following the de Gennes theory[45] or for bulk superconductors.[23] Please note that even without external bias, the term $1/b_0$ exists due to impurities and is usually small.[45]

APPENDIX B: SURFACE COUNTERTERM IN GL EQUATION

For simplicity we consider the one-dimensional problem with a superconductor in the $x>0$ direction. The GL free-energy density reads

$$f(x) = f_0 + \alpha(x)\Psi(x)^2 + \gamma\Psi'(x)^2 + \frac{\beta}{2}\Psi(x)^4, \tag{B1}$$

where $\alpha(x)=\alpha+\frac{\gamma}{4l^2}(\tau_0+x/l)^2$ and $\gamma=\hbar^2/2m$. Searching for a minimum of

$$\delta\int_0^\infty f(x)dx = 0 \tag{B2}$$

with the ansatz $\Psi(x)=\mathcal{C}D_\nu(x)$ with respect to the amplitude $\mathcal{C}$ leads to Eq. (23) with Eq. (25) without counterterms and Eq. (26). This minimum condition can be written also as

$$\begin{aligned} 0 &= \int_0^\infty [\gamma\Psi'^2 + \alpha(x)\Psi^2 + \beta\Psi^4] \\ &= \int_0^\infty [-\gamma\Psi\Psi'' + \alpha(x)\Psi^2 + \beta\Psi^4] - \gamma\Psi(0)\Psi'(0). \end{aligned} \tag{B3}$$

This minimum condition differs from the Lagrange equation of motion as the functional minimization of Eq. (B1),

$$\partial_x\left(\frac{\delta f}{\delta\Psi'}\right) - \frac{\delta f}{\delta\Psi} = 0, \tag{B4}$$

leading to the GL equation

$$-\gamma\Psi'' + \alpha(x)\Psi - \beta\Psi^3 = 0 \tag{B5}$$

just by the surface term $\Psi'(0)\Psi(0)$. For standard GL boundary conditions, $\Psi'(0)=0$, this difference does not matter. With modified GL boundary condition (4), however, we have to add a counterterm to compensate for this artifact, i.e.,

$$f(x) \to f(x) + \gamma\Psi'(0)\Psi(0)\delta(x). \tag{B6}$$

APPENDIX C: DOMAIN-WALL SURFACE ENERGY

Here we outline the derivation of domain-wall parameter (28) without external bias $b\to\infty$ and for the situation of normal-superconducting boundaries as it is usually found in literature.[45,51,52] In terms of Eq. (9), nonlinearized equation (3) reads

$$-\xi^2\psi'' + \frac{\xi^2}{4l^4}(x+\tau_0 l)^2\psi + \psi - \psi^3 = 0. \tag{C1}$$

and domain-wall parameter (27) for $B_a\approx B_c$ is

$$\delta(\infty) = \int_0^\infty dx \left\{ \psi^4 + 2\xi^2 \psi'^2 + \psi^2 \left[\frac{\xi^2}{l^2}(x+\tau_0 l)^2 - 2 \right] \right\}. \tag{C2}$$

One can simplify this expression by noting an additional conservation law valid for one-dimensional GL equations.[55] Multiplying GL equation (C1) by $\psi(x)$ and integrating over x, one gets exactly

$$\int_0^\infty dx \left\{ \xi^2 \left[\frac{1}{2}(x/l+\tau_0)^2 \psi^2 + \psi'^2 \right] - \psi^2 + \psi^4 \right\} = 0. \tag{C3}$$

Subtracting this relation from Eq. (C2), one has the simpler form

$$\delta(\infty) = \int_0^\infty dx \left\{ -\psi(x)^4 + \left[\frac{M(x)}{B_c} \right]^2 \right\}. \tag{C4}$$

The domain wall is characterized by an exponential decay of the magnetic field inside the superconductor and a decay of the superconductor wave function outside. One can calculate the domain-wall parameter for two extreme cases analytically.

In strong type-I superconductivity, $\kappa \ll 1$, no magnetic fields are inside, $M(x) = -B_a$. Approximating $\xi^2/l^2 \sim B_a \approx 0$ and with the boundary condition at the surface $\psi(0)=0$ and deep in the superconductor $\psi(\infty)=1$, linearized equation (7) has a first integral

$$\xi^2 \psi'(x)^2 = \frac{1}{2}[1-\psi(x)]^2, \tag{C5}$$

which can be easily verified by multiplying Eq. (C1) by $2\psi'(x)$ and integrating from 0 to ∞. Taking this first integral [Eq. (C5)] into account, one finds for Eq. (C2)

$$\delta_{\mathrm{I}}(\infty) = \int_0^\infty dx [2\xi^2 \psi'^2 + (1-\psi^2)^2] = 2\int_0^\infty dx (1-\psi^2)^2$$
$$= 2\sqrt{2}\xi \int_0^1 d\psi (1-\psi^2)^2 = \frac{4}{3}\sqrt{2}\xi = 1.89\xi, \tag{C6}$$

where we have used Eq. (C5) from the third to the fourth term once more. We see that in type-I superconductors the surface energy is proportional to the coherence length.

The other case of extreme type-II superconductor is characterized by $\psi \approx 1$ and an exponentially damped magnetic field profile with the London penetration depth λ. Therefore Eq. (C2) becomes

$$\delta_{\mathrm{II}}(\infty) = \int_0^\infty dx [(1-e^{-x/\lambda})^2 - 1] = -\frac{3}{2}\lambda, \tag{C7}$$

and we see that the surface energy is proportional to the London penetration depth and becomes negative, indicating instability. We can combine Eqs. (C6) and (C7),

$$\delta \approx -\lambda \left(\frac{3}{2} - \frac{4\sqrt{2}}{3\kappa} \right), \tag{C8}$$

as an interpolation formula for both type-I and type-II superconductors.[45,51,52]

APPENDIX D: INDUCED MAGNETIC FIELD DUE TO DIAMAGNETIC CURRENTS

1. Self-consistent magnetization

We are now going to investigate the general form of the magnetization provided a profile of the wave function is given. The total induction becomes $B(x,y) = B_a + \mu_0 M(x,y)$ due to the induced magnetization $\mu_0 M(x,y)$, which is determined by the supercurrent $\mathbf{j}$. For the sake of completeness, we discuss also the y dependence.

The external magnetic field and the magnetization are directed in the z direction,

$$[0,0,B_a + \mu_0 M(x,y)] = \mathrm{rot}\, \mathbf{A}, \tag{D1}$$

from which one sees that $A_z = 0$ and the remaining possible dependencies of the vector potential are $A_x(x,y)$ and $A_y(x,y)$ and

$$\frac{\partial A_y}{\partial x} - \frac{\partial A_x}{\partial y} = B_a + \mu_0 M(x,y). \tag{D2}$$

The current is given by

$$\mathbf{j} = (\hbar \mathbf{k} - e\mathbf{A}) \frac{e}{m} |\psi(x,y)|^2 = \frac{1}{\mu_0} \mathrm{rot}\, \mathbf{B} = \left(\frac{\partial M}{\partial y}, -\frac{\partial M}{\partial x}, 0 \right), \tag{D3}$$

from which we get the two equations

$$\frac{\partial M}{\partial y} = -\frac{e^2}{m} |\Psi(x,y)|^2 A_x,$$

$$\frac{\partial M}{\partial x} = -\frac{e^2}{m} |\Psi(x,y)|^2 \left(A_y - \frac{\hbar k}{e} \right). \tag{D4}$$

Eliminating the vector potential in Eq. (D2) with the help of Eq. (D4), we arrive at the differential equation for the magnetization,

$$\frac{e^2 \mu_0}{m} M = \frac{\partial}{\partial x} \left(\frac{1}{|\Psi|^2} \frac{\partial}{\partial x} M \right) + \frac{\partial}{\partial y} \left(\frac{1}{|\Psi|^2} \frac{\partial}{\partial y} M \right), \tag{D5}$$

as the most general equation determining the magnetization profile. It represents a homogeneous linear differential equation of second order, which can be solved for the given geometry and a wave function $\Psi(x,y)$ numerically.

Here we restrict ourselves to a slightly simpler geometry, where we consider superconductors of large size in the y direction; see Fig. 1. This means that the dependence is only $A_y(x)$ and consequently $M(x)$, which means $A_x = 0$ according to Eq. (D4) and further

$$A_y(x) = B_a x + \mu_0 \int_0^x dx' M(x'). \tag{D6}$$

Now we introduce the dimensionless coordinates [Eq. (11)] and

$$|\psi(x)|^2 = \frac{\alpha}{\beta} N D^2(\tau), \tag{D7}$$

where the wave function ψ is given by the parabolic cylinder functions $D^2(\tau) = D^2_{\tilde{\nu}}(\tau)$ of Eq. (12) only in the linearized ansatz, while here D^2 stands for the square of the appropriately scaled general wave function. In these coordinates Eq. (D4) leads then to the integral equation

$$\frac{\mu_0 M(x)}{B_c} = -\frac{N}{\sqrt{2}\kappa} \int_{\tau_0}^{\tau} d\tau' \tau' D^2(\tau') - \frac{N B_c}{\sqrt{2}\kappa B_a} \int_{\tau_0}^{\tau} d\tau' D^2(\tau') \int_{\tau_0}^{\tau'} d\tau'' \frac{\mu_0 M(\tau'')}{B_c}. \tag{D8}$$

Differentiating Eq. (D8) twice and replacing one integral in the resulting equation by the expression obtained by differentiating Eq. (D8) once, we arrive at the differential equation

$$h(\tau) y''(\tau) - h'(\tau) y'(\tau) + a h^2(\tau) y(\tau) = 0,$$

$$y(\tau_0) = 1, \quad y'(\tau_0) = -a\tau_0 h(\tau_0) \tag{D9}$$

for the magnetization,

$$y(\tau) = \frac{\mu_0 M(\tau)}{B_a} + 1, \tag{D10}$$

where we introduced the abbreviations

$$h(\tau) = D^2(\tau),$$

$$a = \frac{N B_c}{\sqrt{2}\kappa B_a}. \tag{D11}$$

Please note that the trivial solution $y=0$ would mean total diamagnetism and complete Meissner effect. We see from the initial conditions in Eq. (D9) that this is ruled out. Instead we have a complicated profile. We can alternatively transform Eq. (D9) by $z(x) = -y'(x)/y(x)h(x)$ also into a Riccati equation,

$$z'(x) - h(x) z^2(x) - a = 0,$$

$$z(\tau_0) = a\tau_0. \tag{D12}$$

2. Approximate form

Since our wave function [Eq. (12)] serves as a variational ansatz, we can restrict the expansion here to terms up to the order $\mathcal{C}^4$. Therefore we obtain from Eq. (D8)

$$\frac{\mu_0 M(x)}{B_c} = -\frac{N}{2\kappa} \int_{\tau_0}^{\tau} d\tau' \tau' D^2_{\tilde{\nu}}(\tau') + \frac{N^2 B_c}{4\kappa^2 B_a} \int_{\tau_0}^{\tau} d\tau' D^2_{\tilde{\nu}}(\tau') \int_{\tau_0}^{\tau'} d\tau'' \tau''(\tau' - \tau'') D^2_{\tilde{\nu}}(\tau'') + \mathcal{O}(N)^3. \tag{D13}$$

This expansion can be alternatively considered as an expansion for large applied fields B_a/B_c and/or large GL parameter κ.

APPENDIX E: INTEGRALS

Here we introduce Eq. (D13) into Eq. (37) to obtain to additional integral expressions beyond Eq. (24) proportional to $\mathcal{B}' N^2$ and $\mathcal{D}' N^3$. In order to maintain legibility, we introduce the integrals

$$\mathcal{H}(\tau) = \int_{\tau_0}^{\tau} d\tau' D^2_{\tilde{\nu}}(\tau'),$$

$$\mathcal{F}(\tau) = \int_{\tau_0}^{\tau} d\tau' \tau' D^2_{\tilde{\nu}}(\tau'),$$

$$\mathcal{G}(\tau) = \int_{\tau_0}^{\tau} d\tau' \tau'^2 D^2_{\tilde{\nu}}(\tau') \tag{E1}$$

and write Gibb free energy (37) with the abbreviation

$$w = d/l + \tau_0 \tag{E2}$$

as

$$\begin{aligned} G = & -l\frac{B_c^2}{2\mu_0}\Bigg[2N\mathcal{A} - N^2\mathcal{B} + \frac{N}{\sqrt{2}\kappa}\int_{\tau_0}^{w} d\tau D^2_{\tilde{\nu}}(\tau) \\ & \times \Bigg(\frac{B_c N^2}{2B_a\kappa^2}\Bigg[\int_{\tau_0}^{\tau} d\tau' \mathcal{F}(\tau')\Bigg]^2 + 2\tau\int_{\tau_0}^{\tau} d\tau' \Bigg\{ -\frac{N}{\sqrt{2}\kappa}\mathcal{F}(\tau') \\ & + \frac{N^2 B_c}{2B_a\kappa^2}\int_{\tau_0}^{\tau'} d\tau'' \mathcal{F}(\tau'')[\mathcal{H}(\tau') - \mathcal{H}(\tau'')] \Bigg\} \Bigg) \\ & - \int_{\tau_0}^{w} d\tau \Bigg\{ \frac{N^2}{2\kappa^2}\mathcal{F}^2(\tau) - \frac{N^3 B_c}{2\sqrt{2}\kappa^3 B_a}\mathcal{F}(\tau) \\ & \times \int_{\tau_0}^{\tau} d\tau' \mathcal{F}(\tau')[\mathcal{H}(\tau) - \mathcal{H}(\tau')] \Bigg\} \Bigg] \\ \equiv & -l\frac{B_c^2}{2\mu_0}(2N\mathcal{A} - N^2(\mathcal{B} + \mathcal{B}') + \mathcal{D}' N^3). \end{aligned} \tag{E3}$$

In the following the procedure will consist of rewriting the integrals into expressions which converge for $w \to \infty$, separating the terms explicitly dependent on w. This is achieved by systematically transforming the multidimensional integrals into integrals containing in each integration a weight of $D^2_{\tilde{\nu}}$.

The additional term in Eq. (E3) proportional to N^2 reads

$$2\kappa^2\mathcal{B}' = \int_{\tau_0}^{w} d\tau \left[\mathcal{F}^2(\tau) + 2\tau D_{\tilde{\nu}}^2(\tau) \int_{\tau_0}^{\tau} d\tau' \mathcal{F}(\tau') \right]. \quad \text{(E4)}$$

Rewriting the first integral

$$\mathcal{F}^2(\tau) = \left[\int_{\tau_0}^{\tau} d\tau' \tau' D_{\tilde{\nu}}^2(\tau') \right]^2 = 2 \int_{\tau_0}^{\tau} d\tau' \tau' D_{\tilde{\nu}}^2(\tau') \int_{\tau_0}^{\tau'} d\tau'' \tau'' D_{\tilde{\nu}}^2(\tau'') \quad \text{(E5)}$$

and interchanging integrations twice according to

$$\int_a^b d\tau \int_a^{\tau} d\tau' = \int_a^b d\tau' \int_{\tau'}^b d\tau, \quad \text{(E6)}$$

we arrive at

$$2\kappa^2\mathcal{B}' = 2 \int_{\tau_0}^{w} d\tau \tau D_{\tilde{\nu}}^2(\tau) \int_{\tau_0}^{\tau} d\tau' \tau' D_{\tilde{\nu}}^2(\tau')(\tau - \tau' + w - \tau) = w\mathcal{F}^2 + \mathcal{I}, \quad \text{(E7)}$$

with

$$\mathcal{I} = -2 \int_{\tau_0}^{w} d\tau \tau D_{\tilde{\nu}}^2(\tau) \mathcal{G}(\tau), \quad \text{(E8)}$$

where we have used Eq. (E5) once more and abbreviate

$$\mathcal{H} \equiv \mathcal{H}(w), \quad \mathcal{F} \equiv \mathcal{F}(w), \quad \mathcal{G} \equiv \mathcal{G}(w). \quad \text{(E9)}$$

Form (E7) shows that $\mathcal{B}'$ is proportional to the thickness of the sample since all remaining integrals converge to a finite value with $\mathcal{O}(\exp(-w))$.

Next we calculate the term $\mathcal{D}'(\sqrt{2}\kappa)^3 B_a/B_c \equiv \tilde{\mathcal{D}}'$ in Eq. (E3) with

$$\tilde{\mathcal{D}}' = \int_{\tau_0}^{w} d\tau D_{\tilde{\nu}}^2(\tau) \left\{ \left[\int_{\tau_0}^{\tau} d\tau' \mathcal{F}(\tau') \right]^2 + 2\tau \int_{\tau_0}^{\tau} d\tau' \tau' \int_{\tau_0}^{\tau'} d\tau'' \mathcal{F}(\tau'')[\mathcal{H}(\tau') - \mathcal{H}(\tau'')] \right\} + 2 \int_{\tau_0}^{w} d\tau \mathcal{F}(\tau) \int_{\tau_0}^{\tau} d\tau' \mathcal{F}(\tau')[\mathcal{H}(\tau) - \mathcal{H}(\tau')]. \quad \text{(E10)}$$

In the first term we apply Eq. (E5) and interchange twice according to Eq. (E6) and in the second term we apply Eq. (E6) once to arrive at

$$\tilde{\mathcal{D}}' = 2 \int_{\tau_0}^{w} d\tau \int_{\tau_0}^{\tau} d\tau' \{ \mathcal{F}(\tau)\mathcal{F}(\tau')[\mathcal{H}(w) - \mathcal{H}(\tau)] + \mathcal{F}(w)\mathcal{F}(\tau') \times [\mathcal{H}(\tau) - \mathcal{H}(\tau')] \}. \quad \text{(E11)}$$

Employing Eq. (E6), it is easy to see that

$$\int_{\tau_0}^{w} d\tau \mathcal{H}(\tau) = w\mathcal{H}(w) - \mathcal{F}(w), \quad \int_{\tau_0}^{w} d\tau \mathcal{F}(\tau) = w\mathcal{F}(w) - \mathcal{G}(w). \quad \text{(E12)}$$

Applying Eqs. (E6) and (E12) on Eq. (E11) yields

$$\tilde{\mathcal{D}}' = \mathcal{H}(w\mathcal{F} - \mathcal{G})^2 - 2w\mathcal{F} \int_{\tau_0}^{w} d\tau \mathcal{H}(\tau)\mathcal{F}(\tau) + 2\mathcal{F} \int_{\tau_0}^{w} d\tau \mathcal{H}(\tau) \times [2\tau\mathcal{F}(\tau) - \mathcal{G}(\tau)] - 2 \int_{\tau_0}^{w} d\tau \mathcal{H}(\tau)\mathcal{F}(\tau)[\tau\mathcal{F}(\tau) - \mathcal{G}(\tau)]. \quad \text{(E13)}$$

Applying Eq. (E6), the first two integrals can be calculated,

$$\int_{\tau_0}^{w} d\tau \mathcal{H}(\tau)[2\tau\mathcal{F}(\tau) - \mathcal{G}(\tau)] = w^2\mathcal{F}H - \mathcal{F}G - w\mathcal{G}H + 2 \int_{\tau_0}^{w} d\tau \tau D_{\tilde{\nu}}^2(\tau)\mathcal{G}(\tau) \quad \text{(E14)}$$

and

$$\int_{\tau_0}^{w} d\tau \mathcal{H}(\tau)\mathcal{F}(\tau) = \mathcal{F}(w\mathcal{H} - \mathcal{F}) - \mathcal{G}H + \mathcal{F}^2 + 2 \int_{\tau_0}^{w} d\tau D_{\tilde{\nu}}^2(\tau)[\mathcal{G}(\tau) - \tau\mathcal{F}(\tau)]. \quad \text{(E15)}$$

Successive applications of Eqs. (E6) and (E12) yield after some straightforward but tedious steps the following:

$$\int_{\tau_0}^{w} d\tau \mathcal{H}(\tau)\mathcal{F}(\tau)[\tau\mathcal{F}(\tau) - \mathcal{G}(\tau)] = \frac{\mathcal{H}}{2}[w\mathcal{F}(w\mathcal{F} - 2\mathcal{G}) + \mathcal{G}^2] - \frac{1}{2} \int_{\tau_0}^{w} d\tau D_{\tilde{\nu}}^2(\tau)[\mathcal{G}(\tau) - \tau\mathcal{F}(\tau)]^2. \quad \text{(E16)}$$

Using Eqs. (E14)–(E16) in Eq. (E13), we arrive finally at

$$\mathcal{D}' = \frac{B_c}{(\sqrt{2}\kappa)^3 B_a}[w\mathcal{F}\mathcal{J} - \mathcal{K}], \quad \text{(E17)}$$

where

$$\mathcal{J} = \mathcal{F}^2 - 2 \int_{\tau_0}^{w} d\tau D_{\tilde{\nu}}^2(\tau)\mathcal{G}(\tau),$$

$$\mathcal{K} = -\int_{\tau_0}^{w} d\tau D_{\tilde{\nu}}^2(\tau)[\tau\mathcal{F}(\tau) - \mathcal{G}(\tau)]^2 + 2\mathcal{F}[\mathcal{F}G + \mathcal{I}]. \quad \text{(E18)}$$

We see that Eqs. (E17) and (E7) are linearly proportional to the thickness of the sample.

[1] R. E. Glover and M. D. Sherrill, Phys. Rev. Lett. **5**, 248 (1960).
[2] V. Matijasevic, S. Bogers, N. Y. Chen, H. M. Appelboom, P. Hadley, and J. Mooij, Physica C **235**, 2097 (1994).
[3] B. I. Smirnov, T. S. Orlova, A. N. Kudymov, M. T. Lanagan, M. P. Chudzik, N. Chen, and K. C. Goretta, Physica C **273**, 255 (1997).
[4] M. Windt, H. Haensel, D. Koelle, and R. Gross, Appl. Phys. Lett. **74**, 1027 (1999).
[5] C. H. Ahn, J. M. Triscone, and J. Mannhart, Nature (London) **424**, 1015 (2003).
[6] D. Matthey, S. Gariglio, and J. M. Triscone, Appl. Phys. Lett. **83**, 3758 (2003).
[7] P. Konsin and B. Sorkin, Phys. Rev. B **58**, 5795 (1998).
[8] X. X. Xi, C. Doughty, A. Walkenhorst, C. Kwon, Q. Li, and T. Venkatesan, Phys. Rev. Lett. **68**, 1240 (1992).
[9] T. Frey, J. Mannhart, J. G. Bednorz, and E. J. Williams, Phys. Rev. B **51**, 3257 (1995).
[10] J. Mannhart, Mod. Phys. Lett. B **6**, 555 (1992).
[11] J. Mannhart, J. Ströbel, G. Bednorz, and C. Gerber, Appl. Phys. Lett. **62**, 630 (1993).
[12] T. Kawahara, N. Sugiuchi, E. Komai, T. Terahima, and Y. Bando, Physica C **276**, 127 (1997).
[13] R. Auer, E. Brecht, K. Herrmann, and R. Schneider, Physica C **299**, 177 (1998).
[14] A. Cassinese, M. Barra, M. Biasiucci, and P. D'Angelo, Macromol. Symp. **234**, 1 (2006).
[15] K. Maki, in *Superconductivity*, edited by R. D. Parks (Dekker, New York, 1969), Vol. 2, Chap. 18.
[16] L. Burlachkov, I. B. Khalfin, and B. Y. Shapiro, Phys. Rev. B **48**, 1156 (1993).
[17] G. A. Ummarino, R. S. Gonelli, and D. Daghero, Int. J. Mod. Phys. B **16**, 1539 (2002).
[18] T. Frey, J. Mannhart, J. G. Bednorz, and E. J. Williams, Phys. Rev. B **51**, 3257 (1995); N. Chandrasekhar, O. T. Valls, and A. M. Goldman, *ibid.* **54**, 10218 (1996) (comment).
[19] M. Salluzzo, A. Cassinese, G. M. De Luca, A. Gambardella, A. Prigiobbo, and R. Vaglio, Phys. Rev. B **70**, 214528 (2004).
[20] N. Chandrasekhar, O. T. Valls, and A. M. Goldman, Phys. Rev. B **49**, 6220 (1994).
[21] G. Montambaux, Phys. Rev. B **54**, R17273 (1996).
[22] K. Morawetz and G. Röpke, Z. Phys. A **355**, 287 (1996).
[23] K. Morawetz, Phys. Rev. B **66**, 172508 (2002).
[24] R. Bertoncini and A. P. Jauho, Phys. Rev. Lett. **68**, 2826 (1992).
[25] W. G. Jenks and L. R. Testardi, Phys. Rev. B **48**, 12993 (1993).
[26] K. T. McCarthy, A. F. Hebard, and S. B. Arnason, Phys. Rev. Lett. **90**, 117201 (2003).
[27] N. Sacchetti, G. Sacerdoti, and G. Sanna, Phys. Lett. **23**, 433 (1966).
[28] G. Paterno, N. Sacchetti, and G. Sacerdoti, Phys. Rev. **185**, 648 (1969).
[29] A. F. Hebard, A. A. Ajuria, and R. H. Eick, Appl. Phys. Lett. **51**, 1349 (1987).
[30] R. Brinkmann, M. Dohlus, D. Trines, A. Novokhatski, M. Timm, T. Weiland, P. Huelsmann, C. T. Rieck, K. Scharenberg, and P. Schmueser, Prepared for the Seventh European Particle Accelerator Conference (EPAC 2000), Vienna, Austria, 26–30 June 2000 (unpublished).
[31] International Workshop on Thin Films and New Ideas for Pushing the Limits of RF Superconductivity, 9–12 October, edited by V. Palmieri (Legnaro National Laboratories INFN, Padua, 2006).
[32] W. J. Tomasch and A. S. Joseph, Phys. Rev. Lett. **12**, 148 (1964).
[33] C. R. Hu and V. Korenman, Phys. Rev. **185**, 672 (1969).
[34] J. Ostenson and D. K. Finnemore, Phys. Rev. Lett. **22**, 188 (1969).
[35] P. L. Indovina, M. Matzeu, S. Onori, and E. Tabet, Solid State Commun. **9**, 1759 (1971).
[36] J. C. Boykin and C. J. Bergeron, Phys. Rev. B **9**, 2084 (1974).
[37] C. J. Bergeron, Phys. Rev. B **30**, 6753 (1984).
[38] G. Eilenberger and V. Ambegaokar, Phys. Rev. **158**, 332 (1967).
[39] B. Y. Shapiro, Solid State Commun. **53**, 673 (1985).
[40] B. Y. Shapiro, Phys. Rev. B **48**, 16722 (1993).
[41] B. Y. Shapiro and I. B. Khalfin, Physica C **209**, 99 (1993).
[42] B. Y. Shapiro, I. B. Khalfin, and L. Burlachkov, Physica B (Amsterdam) **194**, 1893 (1994).
[43] J. Bardeen, Phys. Rev. **94**, 554 (1954).
[44] P. Lipavský, J. Koláček, K. Morawetz, E. H. Brandt, and T. J. Yang, in *Bernoulli Potential in Superconductors*, Lecture Notes in Physics Vol. 733 (Springer, Berlin, 2007).
[45] P. G. de Gennes, *Superconductivity of Metals and Alloys* (Addison-Wesley, New York, 1989).
[46] P. Lipavský, K. Morawetz, J. Koláček, and T. J. Yang, Phys. Rev. B **73**, 052505 (2006).
[47] P. Scotto and W. Pesch, J. Low Temp. Phys. **84**, 301 (1991).
[48] W. Magnus, F. Oberhettinger, and R. P. Soni, *Formulas and Theorems of the Special Functions of Modern Physics* (Springer, Berlin, 1966).
[49] D. Saint-James and P. G. Gennes, Phys. Lett. **7**, 306 (1963).
[50] J. Kirschenbaum, Phys. Rev. B **12**, 3690 (1975).
[51] M. Tinkham, *Introduction to Superconductivity* (McGraw-Hill, New York, 1966).
[52] A. L. Fetter and J. D. Walecka, *Quantum Theory of Many Particle Systems* (McGraw-Hill, New York, 1971).
[53] The pairable charge per Cu atom is $-0.4335e$. Figure 2.16 of Ref. 56 shows the results of Cava *et al.* (Ref. 57), according to which the charge transfer $-0.03e$ from chains to planes per Cu site leads to a decrease in the critical temperature of 30 K. This corresponds to $\frac{\partial \ln T_c}{\partial \ln n}=-4.82$. From Fig. 3 of Ref. 58, we can see that the specific-heat coefficient drops at the same time from 4.4 to 3.0 mJ/g K^2, which gives $\frac{\partial \ln \gamma}{\partial \ln n}=-4.13$. This is only a rough estimate since the specific-heat data include chains, while we need the change in plane only.
[54] W. D. Lee, J. L. Chen, T. J. Yang, and B. S. Chiou, Physica C **261**, 167 (1996).
[55] P. Lipavský, K. Morawetz, J. Koláček, J. J. Mareš, E. H. Brandt, and M. Schreiber, Phys. Rev. B **70**, 104518 (2004).
[56] N. M. Plakida, *High-Temperature Superconductivity* (Springer-Verlag, Berlin, 1995).
[57] R. J. Cava, A. W. Hewat, E. A. Hewat, B. Batlogg, M. Marezio, K. M. Rabe, J. J. Krajewski, W. F. Peck, and L. W. Rupp, Physica C **165**, 419 (1990).
[58] J. W. Loram, K. A. Mirza, J. R. Cooper, and W. Y. Liang, Phys. Rev. Lett. **71**, 1740 (1993).